AIAA JOURNAL
Vol. 48, No. 4, April 2010

Free-Vibration Analysis of Ring-Stiffened Branched Composite Shells of Revolution

Altan Kayran* and Erdem Yavuzbalkan†
Middle East Technical University, 06531 Ankara, Turkey

DOI: 10.2514/1.40489

Application of the multisegment numerical integration technique is extended to the free-vibration analysis of macroscopically anisotropic filament-wound branched shells of revolution with ring stiffeners, considering the variation of the thickness and winding angle. The solution procedure is based on a modified-frequency trial method, which processes on the numerically integrated transformed fundamental shell equations that are obtained in terms of finite exponential Fourier transform of the fundamental shell variables. The full macroscopically anisotropic form of the constitutive relations, including first-order transverse shear deformation and all components of translatory and rotary inertia, are included in the analysis. To handle branched shells of revolution, modifications that are necessary to incorporate junctions are added to the solution procedure. Inclusion of asymmetric circumferential stiffeners, with respect to the middle surface of the shell, into the semi-analytical solution method is demonstrated by presenting two alternative methods of analysis. The present solution methodology also incorporates the variation of the thickness and winding angle along the meridian of filament-wound shells of revolution, with general meridional curvature, by assuming placement of filaments along the geodesic fiber path on the surface of the shell of revolution.

Nomenclature

A_{ij}	=	extensional stiffness coefficients ($i, j = 1, 2, 6$)
As_{ij}	=	transverse shear stiffness coefficients ($i, j = 4, 5$)
B_{ij}	=	bending-stretching coupling stiffness coefficients ($i, j = 1, 2, 6$)
D_{ij}	=	bending stiffness coefficients ($i, j = 1, 2, 6$)
E_1	=	Young's modulus in the fiber direction
E_2	=	Young's modulus transverse to fiber
G_{12}	=	in-plane shear modulus
G_{23}, G_{13}	=	transverse shear moduli
h	=	thickness of the shell wall
h_R	=	offset between the reference surfaces of the shell walls with and without stiffener
$M_{\phi\phi}$, $M_{\theta\theta}$, $M_{\phi\theta}$	=	moment resultants of in-plane normal and shear stresses (per unit length)
$N_{\phi\phi}$, $N_{\theta\theta}$, $N_{\phi\theta}$	=	in-plane normal and shear stress resultants (per unit length)
Q_ϕ, Q_θ	=	transverse shear stress resultant (per unit length)
R	=	distance of a point on the reference surface of the shell of revolution from the shell axis, $R_\theta \sin\phi$
R_θ	=	radius of curvature of the reference surface of the shell in the circumferential θ direction
R_ϕ	=	radius of curvature of the reference surface of the shell in the meridional ϕ direction
t	=	thickness of a single ply of the filament-wound shell of revolution
u_θ^0	=	reference surface displacement of the shell wall in the circumferential direction
u_ϕ^0	=	reference surface displacement of the shell wall along the shell meridian
w^0	=	reference surface displacement of the shell wall in the transverse direction
x	=	axial coordinate of the cylindrical shell
α	=	local winding angle
β	=	angle between the tangents drawn to the reference surfaces at the junction
β_c	=	cone angle
β_ϕ, β_θ	=	rotations of transverse normal about θ and ϕ curvilinear coordinates, respectively.
$\gamma_{\theta\zeta}^0$	=	transverse shear strain in θ-ζ plane
$\gamma_{\phi\zeta}^0$	=	transverse shear strain in ϕ-ζ plane
$\gamma_{\phi\theta}^0$	=	in-plane shear strain of the reference surface
$\varepsilon_{\phi\phi}^0$, $\varepsilon_{\theta\theta}^0$	=	reference surface normal strains along the ϕ and θ curvilinear coordinates, respectively
ζ	=	curvilinear coordinate in the thickness direction, measured from the reference surface
θ	=	circumferential coordinate of the shell of revolution
$\kappa_{\phi\theta}$	=	twisting curvature of the reference surface
$\kappa_{\phi\phi}$, $\kappa_{\theta\theta}$	=	bending curvatures of the reference surface
ν_{12}	=	Poisson's ratio
ρ	=	mass density
ϕ	=	meridional coordinate of the shell of revolution

Introduction

RING-STIFFENED composite branched shells of revolution are widely used in various engineering structures such as rocket fuselages, pressure vessels, submarines, aircraft fuselages, external stores, antenna, etc. Ring stiffeners are not only used to reinforce the whole structure, but they are also used in the connection of the shell segments to construct shells of revolution of one type with a longer meridian and to connect different shells of revolution at the junctions where the shell branches to a different type. Today, due to the availability of various composite manufacturing techniques, it is possible to easily manufacture composite branched shells of revolution. Among the various manufacturing methods, filament-winding is the most commonly used technique to produce geometrically axisymmetric structures [1]. It was probably the first method to be automated and remains one of the most cost-effective methods for mass production today. With the filament-winding technique truncated and closed, shells of revolution with general meridional curvature can be manufactured by using mandrels of the required shape.

Presented as Paper 2114 at the 48th AIAA/ASME/ASCE/AHS/ASC Structures, Structural Dynamics, and Materials Conference, Honolulu, HI, 23–26 April 2007; received 19 August 2008; revision received 6 October 2009; accepted for publication 31 December 2009.

*Associate Professor, Department of Aerospace Engineering; akayran@metu.edu.tr. Associate Member AIAA.

†Graduate Student, Department of Aerospace Engineering; erdemy@metu.edu.tr.

During the filament-winding process, filaments are usually placed in arbitrary orientation with respect to the geometric axis of the shell of revolution. In the present state of the art, the filament-winding process is usually applied by using geodesic paths. For composite conical shells of revolution, it has been shown that when filaments are placed in arbitrary orientation along the geodesic fiber path with respect to the geometric axis of the shell, the thickness and the winding angle (and thus the stiffness coefficients) vary only along the meridional direction [2–4]. In the case of shells of revolution with general meridional curvature, the winding angle and the thickness of the shell of revolution also vary only along the meridional direction if the filaments are placed along the geodesic fiber path [5]. The meridional variation of the winding angle and the thickness of filament-wound shells of revolution brings about additional complexity in the solution of structural mechanics problems pertaining to composite shells of revolution.

Most of the previous work on the study of the free-vibration characteristics of composite shells of revolution has been performed on certain types of shells of revolution without any branch. Some examples from the vast literature include the work of Noor and Peters [6], who used a combination of Fourier series representation in the circumferential direction and a three-field mixed finite element model for the discretization in the meridional direction. Cylindrical and toroidal shells of revolution were analyzed in [6]. A semi-analytical study of laminated cylindrical and conical shells of revolution has been performed by Xi et al. [7], who used conical finite elements and included transverse shear deformation in their analysis, and constant-stiffness coefficients were used in the analysis of conical shells of revolution. Tan [8] presented an efficient substructuring analysis method for predicting the natural frequencies of shells of revolution using the Sturm sequence method in conjunction with the massive substructuring technique. The solution procedure was capable of handling a general type of material property and any kind of boundary condition. Timarci and Soldatos [9] used the state-space concept on the Love-type version of a unified shear deformable shell theory and studied the axisymmetric and flexural vibrations of angle-ply laminated circular cylindrical shells. In [10] a general semi-analytical finite element model was developed for bending, free-vibration, and buckling analyses of laminated shells of revolution, and results were obtained for cylindrical shells. Three-dimensional elasticity theory was used and the equations of motion were obtained by expanding the displacement field and load in the Fourier series in terms of the circumferential coordinate. In these studies, consideration of the variation of the stiffness coefficients with the shell coordinates was not taken into account. It was concluded by Baruch et al. [2] that the stiffness coefficients needed for the analysis of a laminated structure have to be calculated only after taking into account the manufacturing process that can be used to build the structure. The stiffness coefficients of filament-wound laminated shells of revolution strongly depend on the meridional coordinate of the shell of revolution, and therefore the variation of the winding angle and thickness (and thus the variation of the stiffness coefficients) have to be taken into account in the structural analysis of filament-wound composite shells of revolution. In the literature, very few studies considered the variation of the stiffness coefficients in the structural analysis of composite shells of revolution with variable radii of curvature. Among these studies, Korjakin et al. [3] investigated the damped vibrations of laminated conical shells by finite element analysis and incorporated the effect of the variation of the winding angle and thickness on the natural frequencies of laminated conical shells. Park et al. [5] calculated the filament-winding patterns using a semigeodesic-fiber-path equation for an arbitrary surface and incorporated the effect of winding angle and thickness change in the finite element analysis of filament-wound composite structures by the commercial code ABAQUS. A comprehensive study of the effect of the variation of the stiffness coefficients on the buckling behavior of filament-wound conical shells was performed by Goldfield and Arbocz [4]. Recently, Kayran and Yavuzbalkan [11] studied the effect of the variation of stiffness coefficients on the free-vibration characteristics of filament-wound shells by a semi-analytical method based on the numerical integration of the governing equations.

There has not been much study in the literature on the branched composite shells of revolution with ring stiffeners. One study on the combined and stiffened shells of revolution is the work of Sivadas and Ganesan [12], who studied the free-vibration characteristics of cylinder–cone combined shells with stiffeners using a higher-order semi-analytical finite element. Most of the other work on the ring-stiffened composite shells of revolution has been primarily on shells without any branch and on cylindrical shells of revolution. Ruotolo [13] studied the dynamics of shells of revolution reinforced with ring stiffeners and compared the Donnell, Love, Sanders, and Flügge thin-shell theories in the evaluation of natural frequencies of cylinders stiffened with rings. In [13] results were obtained for isotropic and specially orthotropic cylinders that were simply supported at the edges. Xiang et al. [14] presented an analytical method based on the state-space technique and domain-decomposition approach to determine the natural frequencies of isotropic cylindrical shells having multiple intermediate ring supports and various combinations of end-support conditions. Wang and Lin [15] presented an analytical methodology for the vibration analysis of ring-stiffened cross-ply laminated cylindrical shells and studied the effect of inner and outer rings on natural frequencies of ring-stiffened cross-ply laminated cylindrical shells. Pan et al. [16] conducted a study on the free-vibration analysis of ring-stiffened thin circular cylindrical shells with arbitrary boundary conditions.

The main objective of the current paper is to present a methodology based on numerical integration technique to investigate the free-vibration characteristics of filament-wound branched shells of revolution with ring stiffeners. Multisegment numerical integration technique [17] is combined with a modified-frequency trial method, and discrete and continuous variation of the shell properties along the meridian of the shell of revolution is included in the analysis. Thus, the application of the multisegment numerical integration technique is extended to the free-vibration analysis of anisotropic branched shells of revolution and to the analysis of anisotropic branched shells of revolution with ring stiffeners that are placed asymmetrically with respect to the middle surface of the shell of revolution. The method of solution is applicable to any linear shell theory, but in the present study, first-order shear deformation theory based on Reissner–Naghdi shell equations [18] is used. To handle branched shells of revolution, modifications that are necessary to incorporate junctions are added to the solution procedure. Two alternative methods are demonstrated for the inclusion of ring stiffeners into the numerical-integration-based free-vibration analysis. Ring stiffeners are modeled as shell segments with different thickness and material properties, and it is assumed that perfect bonding exists between the shell wall and the ring stiffeners. Since first-order transverse shear deformation theory is used, moderately thick ring stiffeners could be modeled. It is assumed that composite branched shells of revolution with ring stiffeners are manufactured by the filament-winding process by placing filaments along the geodesic fiber path on the surface of the shell of revolution. Therefore, the variation of the winding angle and the thickness along the meridian of the branched shell of revolution is also included in the numerical-integration-based method of free-vibration analysis. It should be noted that numerical integration method of analysis is basically a semi-analytical procedure with the inherent advantageous features of the applicability to any linear shell theory and to general shells of revolution with no restriction on the type of boundary conditions at two ends of the shell. Numerical-integration-based solution technique especially presents significant advantages for the analysis of shells of revolution with variable properties along the meridian of the shell.

Governing Equations of Anisotropic Shells of Revolution

In this section, governing equations of free vibration of anisotropic shells of revolution will be reviewed briefly to build the foundation for the description of the extension of the method of solution to branched anisotropic shells of revolution with ring stiffeners. Figure 1 shows the geometry notation used for a shell of revolution.

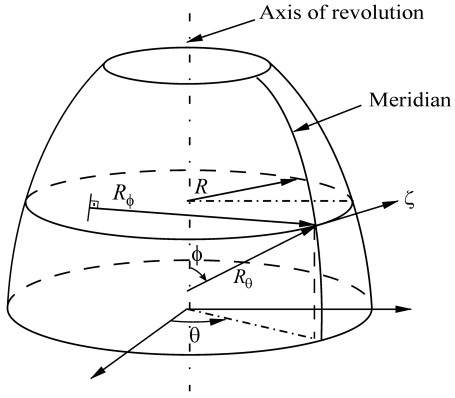

Fig. 1 Geometry and coordinate system of shell of revolution.

Figure 1 shows that the reference surface of the shell of revolution is characterized by two radii of curvature, R_ϕ and R_θ, in the meridional and circumferential directions, respectively. The spatial position of a representative point in the shell wall is defined by the independent coordinates ϕ, θ, and ζ.

The starting point in the application of the numerical integration technique for the solution of the free-vibration problem of a shell of revolution is to express the equations governing the free vibration as a system of partial differential equations given in the form of Eq. (1) [11,19]:

$$\frac{\partial}{\partial\phi}\{\psi(\phi,\theta,t)\} = f\left(\{\psi(\phi,\theta,t)\}, \frac{\partial}{\partial\theta}(\{\psi(\phi,\theta,t)\}), \frac{\partial^2}{\partial^2\theta}(\{\psi(\phi,\theta,t)\})\right) \quad (1)$$

where $\{\psi\}$ is a vector representing the fundamental shell variables that enter into the appropriate boundary conditions on a rotationally symmetric edge of the shell of revolution, and for the Reissner–Naghdi improved shell theory, they are given by [20,21]

$$\{\psi(\phi,\theta,t)\} = \{w^0, u^0_\phi, u^0_\theta, \beta_\phi, \beta_\theta, Q_\phi, N_{\phi\phi}, N_{\phi\theta}, M_{\phi\phi}, M_{\phi\theta}\}^T \quad (2)$$

The first half of the vector $\{\psi\}$ consists of the reference-plane displacements and rotations and the second half consists of the stress and moment resultants that are defined in an appropriate manner [20,22].

The system of equations given by Eq. (1) is derived by the complex manipulation of three set of equations that are the strain-displacement relations of the Reissner–Naghdi shell theory [20,21], dynamic equilibrium equations [20,21], and full anisotropic form of the constitutive relations relating the stress and moment resultants to midsurface strains and curvatures of the laminated shell wall [22]. For laminated composite structures, full anisotropic form of the constitutive relations relating the stress and moment resultants to midsurface strains $(\varepsilon^0_{\phi\phi}, \varepsilon^0_{\theta\theta}, \gamma^0_{\phi\theta})$ and curvatures $(\kappa_{\phi\phi}, \kappa_{\theta\theta}, \kappa_{\phi\theta})$ are given in matrix form by Eq. (3) [22]:

$$\begin{Bmatrix} N_{\phi\phi} \\ N_{\theta\theta} \\ N_{\phi\theta} \\ M_{\phi\phi} \\ M_{\theta\theta} \\ M_{\phi\theta} \end{Bmatrix} = \begin{bmatrix} A_{11} & A_{12} & A_{16} & B_{11} & B_{12} & B_{16} \\ A_{12} & A_{22} & A_{26} & B_{12} & B_{22} & B_{26} \\ A_{16} & A_{26} & A_{66} & B_{16} & B_{26} & B_{66} \\ B_{11} & B_{12} & B_{16} & D_{11} & D_{12} & D_{16} \\ B_{12} & B_{22} & B_{26} & D_{12} & D_{22} & D_{26} \\ B_{16} & B_{26} & B_{66} & D_{16} & D_{26} & D_{66} \end{bmatrix} \begin{Bmatrix} \varepsilon^0_{\phi\phi} \\ \varepsilon^0_{\theta\theta} \\ \gamma^0_{\phi\theta} \\ \kappa_{\phi\phi} \\ \kappa_{\theta\theta} \\ \kappa_{\phi\theta} \end{Bmatrix} \quad (3)$$

where N_{ij} terms represent force per unit length, and M_{ij} terms represent moment per unit length. The stiffness coefficients are expressed in the usual manner [22]. Transverse shear stress resultants are related to transverse shear strains $(\gamma^0_\theta, \gamma^0_\phi)$ by Eq. (4):

$$\begin{Bmatrix} Q_\theta \\ Q_\phi \end{Bmatrix} = \begin{bmatrix} As_{44} & As_{45} \\ As_{45} & As_{55} \end{bmatrix} \begin{Bmatrix} \gamma^0_\theta \\ \gamma^0_\phi \end{Bmatrix} \quad (4)$$

In Eq. (4) the transverse shear stiffness coefficients are given by [22]

$$(As_{44}, As_{45}, As_{55}) = \sum_{k=1}^{N_L} \int_{h_{k-1}}^{h_k} (\bar{Q}^{(k)}_{44}, \bar{Q}^{(k)}_{45}, \bar{Q}^{(k)}_{55}) f(\zeta)\, \mathrm{d}\zeta \quad (5)$$

where

$$f(\zeta) = \frac{5}{4}\left[1 - 4\left(\frac{\zeta}{h}\right)^2\right] \quad (6)$$

In Eq. (5) it is assumed that the transverse shear stress has a parabolic distribution across the shell wall. A factor of 5/4 multiplies the distribution function used by Whitney [23] so that the shear factor calculated for the layered anisotropic shell wall can be consistent with the established shear factor from the previous work of Reissner [18] and Mindlin [24] for the homogenous case.

In the derivation process of dynamic equilibrium equations, application of Hamilton's principle also generates conditions on the boundary displacements and rotations, and boundary stress and moment resultants that are applied at the edge of a shell of revolution at a constant meridional coordinate ϕ. For the free-vibration problem, boundary conditions are given by setting one of the variables, given inside the parentheses of the shell variable pairs in Eq. (7), to zero [20]:

$$(N_{\phi\phi}, u^0_\phi), (N_{\phi\theta}, u^0_\theta), (Q_\phi, w^0), (M_{\phi\phi}, \beta_\phi), (M_{\phi\theta}, \beta_\theta) = 0 \quad (7)$$

For a laminated composite structure when the full anisotropic form of the constitutive relations is used, the existence of full coupling stiffness coefficients precludes the uncoupling of fundamental system of shell equations, describing the symmetric and antisymmetric responses with respect to the circumferential coordinate θ, by the classical sine or cosine Fourier decomposition of the fundamental shell variables. Therefore, to accomplish the uncoupling of the circumferential coordinate from the fundamental system of equations, finite exponential Fourier transform of each fundamental variable is taken. In the following, it is assumed that for the free-vibration analysis, the time dependence of each quantity in synchronous motion appears in a factor $e^{i\omega t}$, where ω is the natural frequency. Therefore, time variable is eliminated from the definition of the fundamental variable vector. Equation (8) shows the exponential Fourier transform of the fundamental variable vector $\{\psi\}$:

$$\frac{1}{2\pi}\int_0^{2\pi} \{\psi(\phi,\theta)\} e^{-in\theta} = \{\psi_{nc}(\phi)\} - i\{\psi_{ns}(\phi)\} \quad (8)$$

where

$$\{\psi_{nc}(\phi)\} = \frac{1}{2\pi}\int_0^{2\pi} \{\psi(\phi,\theta)\} \cos n\theta\, \mathrm{d}\theta \quad (9)$$

$$\{\psi_{ns}(\phi)\} = \frac{1}{2\pi}\int_0^{2\pi} \{\psi(\phi,\theta)\} \sin n\theta\, \mathrm{d}\theta \quad (10)$$

The actual physical fundamental shell variables are constructed by the complex Fourier series given in Eq. (11):

$$\{\psi(\phi,\theta)\} = \sum_{-\infty}^{+\infty} \{\psi_n(\phi)\} e^{in\theta} \quad (11)$$

It is evident from Eq. (8) that application of finite exponential Fourier transform results in doubling of the number of fundamental variables. Finite exponential Fourier transform of the fundamental system of partial differential equations (1) yields a system of ordinary differential equations in terms of the transformed fundamental shell variables:

$$\frac{\mathrm{d}}{\mathrm{d}\phi}\{\psi\} = \frac{\mathrm{d}}{\mathrm{d}\phi}\begin{Bmatrix} \psi^{(1)}(\phi) \\ \psi^{(2)}(\phi) \end{Bmatrix}_{20\times1} = [K(n,\omega,\phi)]_{20\times20} \begin{Bmatrix} \psi^{(1)}(\phi) \\ \psi^{(2)}(\phi) \end{Bmatrix}_{20\times1} \quad (12)$$

where n is the circumferential wave number, and the partitions of the fundamental variable vector are given by

$$\{\psi^{(1)}(\phi)\} = \{w^0_{nc}, w^0_{ns}, u^0_{\phi nc}, u^0_{\phi ns}, u^0_{\theta nc}, u^0_{\theta ns}, \beta_{\phi nc}, \beta_{\phi ns}, \beta_{\theta nc}, \beta_{\theta ns}\}^T \tag{13}$$

$$\{\psi^{(2)}(\phi)\} = \{Q_{\phi nc}, Q_{\phi ns}, N_{\phi\phi nc}, N_{\phi\phi ns}, N_{\phi\theta nc}, N_{\phi\theta ns}, M_{\phi\phi nc}, M_{\phi\phi ns}, M_{\phi\theta nc}, M_{\phi\theta ns}\}^T \tag{14}$$

The fundamental variable vector ψ is partitioned such that the first half consists of the transformed displacements and rotations, and the second half consists of the transformed stress and moment resultants. In Eqs. (13) and (14), variables with subscript c refer to symmetric modes with respect to the tangential coordinate θ of the shell of revolution, and subscript s refers to antisymmetric modes. The elements of the coefficient matrix K depend on the circumferential wave number, natural frequency, and meridional coordinate ϕ. The dependency of the coefficient matrix on the thickness, radii of curvature, and stiffness coefficients appears through the meridional coordinate ϕ. For a general shell of revolution with arbitrary change of geometric and material properties along the meridian of the shell, thickness, radii of curvature, and stiffness coefficients depend on the meridional coordinate ϕ. The elements of the coefficient matrix K for a general shell of revolution with full macroscopically anisotropic laminated shell wall are given in the recent work of Kayran and Yavuzbalkan [11], and they will not be repeated here, for brevity. Application of the finite exponential Fourier transform to Eq. (7) results in doubling of the number of boundary conditions that are defined in terms of cosine and sine parts of the Fourier transform of the fundamental shell variables. Thus, for the first-order shear deformation theory, 10 boundary conditions need to be applied at an edge of the shell of revolution. The fundamental system of equations (12) together with the finite exponential Fourier transform of the boundary conditions (7) specified at the two boundary edges of an anisotropic shell of revolution completely define an eigenvalue problem.

Variation of Winding Angle and Thickness of Filament-Wound Shells of Revolution

In filament-winding operation, fibers are placed along arbitrary paths on the surface of a mandrel that is used to manufacture the required shell of revolution. Common practice in filament-winding operation is to place the fibers along the geodesic path on the surface of the shell of revolution. The geodesic path connects two points along the shortest distance on the surface of a shell of revolution. Placement of fibers along the geodesic path results in a stable system, and hence no friction is required to keep the fiber from slipping. For a general shell of revolution that is filament-wound by placing the fibers along the geodesic path, the local winding angle changes along the axis of the shell of revolution. The change of the winding angle is given by Eq. (15) [5,11]:

$$\sin\alpha = \sin\alpha_1 \frac{\sin\phi_1}{\sin\phi} = \sin\alpha_1 \frac{R_1}{R} \tag{15}$$

where α is the local winding angle at (ϕ, R) and α_1 is the initial winding angle at the location (ϕ_1, R_1). Based on the initial the winding angle at the starting edge of the winding operation, the winding angle at any meridional location ϕ can be determined from Eq. (15).

In filament-winding operation, any unit length of the filament brings with itself the same amount of matrix material, and the number of filaments at any cross section is always constant. Thus, it follows that the thickness of a general filament-wound shell of revolution, at any axial location, can be calculated from Eq. (16) [4,5,11]:

$$t = t_1 \frac{R_1 \cos\alpha_1}{R\cos\alpha} \tag{16}$$

where t is the local thickness of the single ply at location (ϕ, R), α is the local winding angle, and t_1 is the thickness of the single ply at location (ϕ_1, R_1), where the winding angle is α_1. Based on the initial thickness of the single ply at the starting edge of the winding operation, the thickness of the single ply at any meridional location ϕ can be determined from Eq. (16). The variation of the winding angle and the thickness of the filament-wound general shell of revolution given by Eqs. (15) and (16) also cause the stiffness coefficients A_{ij}, B_{ij}, and D_{ij} to vary along the meridian of the shell continuously. Therefore, the elements of the coefficient matrix K [Eq. (12)] vary continuously along the meridian of the shell of revolution. For filament-wound shells of revolution with constant radii of curvature, such as a cylindrical shell of revolution, the local winding angle and thickness remains constant and the elements of the coefficient matrix K are also constant.

Extension of the Numerical Integration Technique to Branched Shells of Revolution

Method of Solution

In this section the extension of the multisegment numerical integration technique to the free-vibration analysis of filament-wound branched shells of revolution will be explained. In the multisegment numerical integration technique, the shell is divided into M number of segments in the meridional direction and the solution to Eq. (12) can be written as [17]

$$\{\psi(\phi)\} = [T_i(\phi)]\{\psi(\phi_i)\} \qquad (i = 1, 2, \ldots, M) \tag{17}$$

where the transfer matrices T_i are obtained from the initial-value problems defined in each segment i by

$$\frac{\mathrm{d}}{\mathrm{d}\phi}[T_i(\phi)] = [K(n, \omega, \phi)][T_i(\phi)] \tag{18}$$

$$[T_i(\phi_i)] = [I] \tag{19}$$

At the start of each shell segment, the transfer matrices are initialized to identity matrices.

The initial step in the solution procedure is to integrate Eq. (18), subject to initial conditions Eq. (19), in each shell segment and store the elements of the transfer matrices at the end of each shell segment. For a particular circumferential wave number and trial frequency, Eq. (18) is numerically integrated and the arbitrary variation of the geometric and material properties of the shell of revolution is handled during the numerical integration process. In the current study, numerical integration of Eq. (18) within each shell segment is performed by the International Mathematical and Statistical Library subroutine `DIVPAG` that uses a user-supplied subroutine in which all the elements of the coefficient matrix K are given. Therefore, as long as the discrete or continuous variation of the elements of the coefficient matrix along the meridian of the branched shell of revolution is coded accordingly, arbitrary variation of the shell properties can be handled, provided that the transformation of the fundamental shell variables are done properly at the junctions where the shell branches into a different type. In the current study the branched shell of revolution is assumed to be manufactured by the filament-winding process, such that the winding angle and the thickness vary according to Eqs. (15) and (16). Thus, the stiffness coefficients also vary continuously along the meridian of the shell of revolution. However, the continuous variation of the stiffness coefficients and the thickness does not generate additional difficulty in the numerical integration of Eq. (18) in each shell segment.

The solution procedure for the anisotropic branched shell of revolution will be demonstrated for a branched shell consisting of two distinct regions. Figure 2 shows the reference surface of a branched shell of revolution with two distinct regions $S1$ and $S2$. In Fig. 2 j denotes the location of the junction at which the shell geometry branches into a different type. $T1$ and $T2$ denote the tangents drawn at the junction j on the reference surface of the branched shell of revolution with distinct regions $S1$ and $S2$.

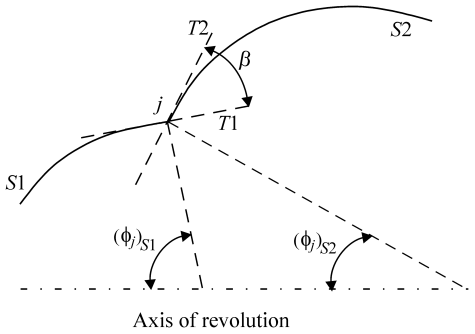

Fig. 2 Generator of the reference surface of a branched shell of revolution.

The initial-value problems defined by Eqs. (18) and (19) can be written in two distinct shell regions $S1$ and $S2$ as

$$\frac{\mathrm{d}}{\mathrm{d}\phi}[T_i(\phi)]_{S1} = [K(n,\omega,\phi)]_{S1}[T_i(\phi)]_{S1} \qquad [T_i(\phi_i)]_{S1} = [I] \tag{20}$$

$$\frac{\mathrm{d}}{\mathrm{d}\phi}[T_i(\phi)]_{S2} = [K(n,\omega,\phi)]_{S2}[T_i(\phi)]_{S2} \qquad [T_i(\phi_i)]_{S2} = [I] \tag{21}$$

where any changes in the geometry and material properties of the two different shell types are assumed to be reflected in the coefficient matrices K_{S1} and K_{S2}. The fundamental shell variable vector $\{\psi\}$ is also defined in two distinct shell regions $S1$ and $S2$ as $\{\psi\}_{S1}$ and $\{\psi\}_{S2}$. After the numerical integration of Eqs. (20) and (21) is accomplished, the transfer matrices are stored at the end of each shell segment. To proceed with the free-vibration analysis of the branched shell of revolution, the continuity relations of the fundamental variables at the end of each shell segment must be written. At the junction of the branched shell of revolution, the fundamental variables of the shell $S1$ and the fundamental variables of the shell $S2$ must obey the following transformation relations:

$$\begin{aligned} \{\psi^{(1)}(\phi_j)\}_{S2} &= [\mathrm{TR}]_{10\times 10}\{\psi^{(1)}(\phi_j)\}_{S1} \\ \{\psi^{(2)}(\phi_j)\}_{S2} &= [\mathrm{TR}]_{10\times 10}\{\psi^{(2)}(\phi_j)\}_{S1} \end{aligned} \tag{22}$$

where the transformation matrix TR transforms the partitioned vectors given by Eqs. (13) and (14). The nonzero coefficients of the transformation matrix are given in the Appendix. The coefficients of the transformation matrix are obtained by expressing the elements of the partitioned fundamental variable vectors $\psi^{(1)}$ and $\psi^{(2)}$ of the shell $S2$, in terms of the elements of the partitioned fundamental variable vectors of the shell $S1$ at the junction. The continuity relations are expressed over the whole span of the branched shell of revolution by writing out Eq. (17) in each shell segment together with the transformation relations at the junction [Eq. (22)]:

$$\begin{Bmatrix} \psi^{(1)}(\phi_{i+1}) \\ \psi^{(2)}(\phi_{i+1}) \end{Bmatrix}_{S1} = \begin{bmatrix} T_i^{(1)}(\phi_{i+1}) & T_i^{(2)}(\phi_{i+1}) \\ T_i^{(3)}(\phi_{i+1}) & T_i^{(4)}(\phi_{i+1}) \end{bmatrix} \begin{Bmatrix} \psi^{(1)}(\phi_i) \\ \psi^{(2)}(\phi_i) \end{Bmatrix}_{S1} \quad (i = 1, 2, \ldots, j-1) \tag{23}$$

$$\begin{Bmatrix} \psi^{(1)}(\phi_j) \\ \psi^{(2)}(\phi_j) \end{Bmatrix}_{S2} = \begin{bmatrix} \mathrm{TR} & 0 \\ 0 & \mathrm{TR} \end{bmatrix}_i \begin{Bmatrix} \psi^{(1)}(\phi_j) \\ \psi^{(2)}(\phi_j) \end{Bmatrix}_{S1} \qquad (i = j) \tag{24}$$

$$\begin{Bmatrix} \psi^{(1)}(\phi_{i+1}) \\ \psi^{(2)}(\phi_{i+1}) \end{Bmatrix}_{S2} = \begin{bmatrix} T_i^{(1)}(\phi_{i+1}) & T_i^{(2)}(\phi_{i+1}) \\ T_i^{(3)}(\phi_{i+1}) & T_i^{(4)}(\phi_{i+1}) \end{bmatrix}_{S2} \begin{Bmatrix} \psi^{(1)}(\phi_i) \\ \psi^{(2)}(\phi_i) \end{Bmatrix}_{S2} \quad (i = j, \ldots, M) \tag{25}$$

For shells of revolution without a branch, Eqs. (20) and (21) reduce to a single equation, β is zero, and the continuity relations are valid for a single shell of revolution. In this case the transformation matrix reduces to an identity matrix and the transformation relation given by Eq. (24) is a trivial relation. For the branched shell of revolution that has a common tangent at the junction, β is again zero, but Eqs. (20) and (21) remain as two distinct equations in this case, since the elements of the coefficient matrices K_{S1} and K_{S2} may have different expressions, depending on the shell types. In this case, Eq. (24) again becomes a trivial relation.

For computational ease, the rows of the fundamental variable vector ψ at both ends of the shell, ϕ_1 and ϕ_{M+1}, are adjusted such that for the anisotropic branched shell of revolution, the first 10 elements of $\{\psi(\phi_1)\}_{S1}$ and the last 10 elements of $\{\psi(\phi_{M+1})\}_{S2}$ are the prescribed boundary conditions. In the following, to keep the uniformity of the notation used for the partitioned fundamental variable vector, the boundary conditions are also represented by the same vector notation defined by Eqs. (13) and (14). Therefore, the boundary condition at the ends of the branched shell of revolution is expressed by

$$\{\psi^{(1)}(\phi_1)\}_{S1} = \{\psi^{(2)}(\phi_{M+1})\}_{S2} = 0 \tag{26}$$

Continuity relations (23–25) constitute a system of linear homogenous matrix equations with $2M$ unknown partitioned fundamental variable vectors. After writing out Eqs. (23–25) in each shell segment i separately, the whole equation set is brought into an upper triangular matrix equation by Gauss elimination:

$$\begin{bmatrix} E_1 & -I & 0 & & & & & & & & 0 \\ 0 & C_1 & -I & 0 & & & & & & & 0 \\ & \ddots & \ddots & \ddots & \ddots & & & & & & \vdots \\ & & 0 & E_{j-1} & -I & 0 & & & & & 0 \\ & & & 0 & C_{j-1} & -I & 0 & & & & 0 \\ & & & & 0 & E_Z & -I & 0 & & & 0 \\ & & & & & 0 & C_Z & -I & 0 & & 0 \\ & & & & & & 0 & E_j & -I & 0 & 0 \\ & & & & & & & 0 & C_j & -I & 0 \\ & & & & & & & & \ddots & \ddots & \vdots \\ & & & & & & & & & 0 & E_M & -I \\ 0 & \cdots & 0 & 0 & 0 & 0 & 0 & 0 & 0 & 0 & 0 & C_M \end{bmatrix} \begin{Bmatrix} \psi_{S1}^{(2)}(\phi_1) \\ \psi_{S1}^{(1)}(\phi_2) \\ \vdots \\ \psi_{S1}^{(2)}(\phi_{j-1}) \\ \psi_{S1}^{(1)}(\phi_j) \\ \psi_{S1}^{(2)}(\phi_j) \\ \psi_{S2}^{(1)}(\phi_j) \\ \psi_{S2}^{(2)}(\phi_j) \\ \psi_{S2}^{(1)}(\phi_{j+1}) \\ \vdots \\ \psi_{S2}^{(2)}(\phi_M) \\ \psi_{S2}^{(1)}(\phi_{M+1}) \end{Bmatrix} = 0 \tag{27}$$

where E_i and C_i represent the 10×10 submatrices that are expressed in terms of the partitioned transfer matrices $T_i^{(1,2,3,4)}$. In the first shell, $S1$ submatrices E_i and C_i are calculated from

$$E_1 = T_1^{(2)} \tag{28}$$

$$C_1 = T_1^{(4)} E_1^{-1} \tag{29}$$

$$E_i = T_i^{(2)} + T_i^{(1)} C_{i-1}^{-1} \qquad (i = 2, 3, \ldots, j-1) \tag{30}$$

$$C_i = (T_i^{(4)} + T_i^{(3)} C_{i-1}^{-1}) E_i^{-1} \qquad (i = 2, 3, \ldots, j-1) \tag{31}$$

The transition matrices E_Z and C_Z are calculated from

$$E_Z = [\mathrm{TR}] C_{j-1}^{-1} \tag{32}$$

$$C_Z = [\mathrm{TR}] E_Z^{-1} \tag{33}$$

In the second shell, $S2$ submatrices E_i and C_i are calculated from

$$E_j = T_j^{(2)} + T_j^{(1)} C_Z^{-1} \tag{34}$$

$$C_j = (T_j^{(4)} + T_j^{(3)} C_Z^{-1}) E_Z^{-1} \tag{35}$$

$$E_i = T_i^{(2)} + T_i^{(1)} C_{i-1}^{-1} \qquad (i = j+1, \ldots, M) \tag{36}$$

$$C_i = (T_i^{(4)} + T_i^{(3)} C_{i-1}^{-1}) E_i^{-1} \qquad (i = j+1, \ldots, M) \tag{37}$$

For the anisotropic branched shell of revolution, the natural frequency is determined from the last row of Eq. (27) by requiring the determinant of the coefficient matrix C_M to vanish. Solution of the natural frequencies is accomplished by evaluating the determinant of the characteristic matrix for incremented values of frequency estimates within a frequency range of interest. When the finite exponential Fourier transform of the fundamental shell equations was used, it was observed that determinant of the characteristic matrix does not change sign; rather, it is always positive and vanishes at the eigenvalue [11]. Therefore, a slope change detection algorithm in combination with inverse interpolations was devised to extract the natural frequency. The method essentially relies on checking the slope change of the determinant of the characteristic matrix and detecting an interval at which a natural frequency resides. Once an interval is determined, natural frequency is extracted by successive inverse interpolations. The details of the natural frequency extraction algorithm are described in [11]. It should be noted that extension of the multisegment numerical integration technique to the free-vibration analysis of branched shells of revolution is simply accomplished by defining the transformation matrices TR at each junction j and modifying Eq. (27) by inserting new rows $2j-1$ and $2j$, which include the transition matrices E_Z and C_Z.

For each natural frequency determined, the partitioned fundamental variable vector $\psi_{S2}^{(1)}(\phi_{M+1})$ at the end of the branched shell of revolution is determined up to an arbitrary constant. The remaining unknown fundamental variables at the end of each shell segment of distinct shell regions $S1$ and $S2$ are then calculated successively from

$$\psi_{S2}^{(2)}(\phi_M) = E_M^{-1} \psi_{S2}^{(1)}(\phi_{M+1}) \tag{38}$$

$$\psi_{S2}^{(1)}(\phi_{M-i+1}) = C_{M-i}^{-1} \psi_{S2}^{(2)}(\phi_{M-i+1}) \qquad (i = 1, 2, \ldots, M-j) \tag{39}$$

$$\psi_{S2}^{(2)}(\phi_{M-i}) = E_{M-i}^{-1} \psi_{S2}^{(1)}(\phi_{M-i+1}) \qquad (i = 1, 2, \ldots, M-j) \tag{40}$$

$$\psi_{S2}^{(1)}(\phi_j) = C_Z^{-1} \psi_{S2}^{(2)}(\phi_j) \tag{41}$$

$$\psi_{S1}^{(2)}(\phi_j) = E_Z^{-1} \psi_{S2}^{(1)}(\phi_j) \tag{42}$$

$$\psi_{S1}^{(1)}(\phi_{j-i+1}) = C_{j-i}^{-1} \psi_{S1}^{(2)}(\phi_{j-i+1}) \qquad (i = 1, 2, \ldots, j-1) \tag{43}$$

$$\psi_{S1}^{(2)}(\phi_{j-i}) = E_{j-i}^{-1} \psi_{S1}^{(1)}(\phi_{j-i+1}) \qquad (i = 1, 2, \ldots, j-1) \tag{44}$$

At the junction ϕ_j, the elements of the partitioned transformed fundamental variable vector ψ are calculated in each distinct shell of revolution ($S1$ and $S2$), successively, from Eq. (40) for $i = M - j$, Eqs. (41) and (42), and Eq. (43) for $i = 1$. Therefore, at the junction, there are two fundamental variable vectors that are defined with respect to the reference surfaces of distinct shells of revolution, $S1$ and $S2$. The variation of all the transformed fundamental shell variables along the meridian of the shell of revolution can be determined from Eqs. (38–44). The physical fundamental shell variables can then be determined by using the cosine and sine parts of the Fourier transform of the fundamental shell variables in the complex Fourier series representation equation (11) for the particular circumferential vibration mode that is analyzed.

Verification Study

Application of the multisegment numerical integration technique is first demonstrated for the cylinder–cone combination shown in Fig. 3, which shows the reference surface of the branched shell of revolution. The lengths of the meridian of the cylindrical and conical parts are denoted by L_{S1}, and L_{S2}, respectively. The shell variables are defined with respect to the reference surfaces of the distinct shell regions, and in accordance with this definition, the lateral displacements w_{S1}^0 and w_{S2}^0 are shown perpendicularly to the reference surface of the shell.

In the verification study, no change of the winding angle and the thickness of the conical shell are considered, and constant-stiffness coefficients are used. The particular cylinder–cone combination is assumed to be composed of two plies with the following geometrical and material properties.

Geometric properties are cylinder radius $R = 0.1$ m and axial lengths of the cylinder and the cone of $L_{S1} = L_{S2} \times \cos\beta_c = 0.4$ m. Ply material properties are Young's modulus in the fiber direction, $E_1 = 213.74$ GPa; Young's modulus transverse to fiber, $E_2 =$ 18.62 GPa; shear moduli $G_{12} = G_{13} = 5.171$ GPa and $G_{23} =$ 4.137 GPa; Poisson's ratio $\nu_{12} = 0.28$; mass density $\rho =$ 2051.88 kg/m^3; fiber orientation and stacking sequence of 0°/45°; and ply thickness of 1 mm.

The branched shell of revolution is assumed to be free at the left end of the cylinder and clamped at the right end of the cone. Free-vibration analysis is performed for different cone angles β_c in the range of 0–30°. The results obtained by the numerical-integration-based method are compared with the results of finite element solution, which is performed by Nastran [25] using the isoparametric curved thin-shell element QUAD8, which contains four corner grid points and four edge grid points. Layer materials are defined as two-dimensional orthotropic materials, and transverse shear behavior is included in the material definition. The comparison of the variation of the scaled nondimensional fundamental natural frequency W with the cone angle determined by the present method and the finite element solution, which uses the Lanchzos algorithm, is presented in

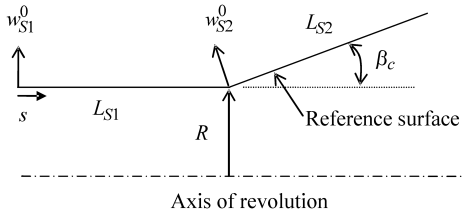

Fig. 3 Generator of the reference surface of the cylinder–cone combination.

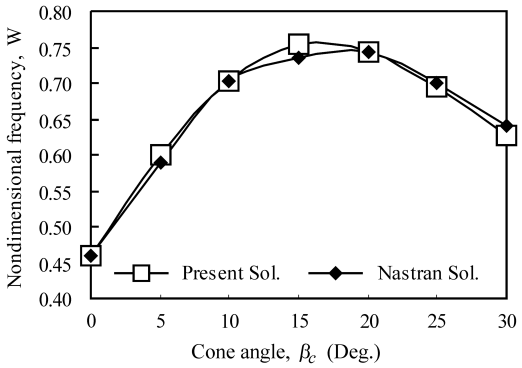

Fig. 4 Fundamental frequency versus cone angle for the cylinder–cone combination ($n = 1$).

Fig. 4 for $n = 1$. The scaled nondimensional frequency W is given by Eq. (45):

$$W = \omega h \sqrt{\rho / E_{11}} \times 1000 \tag{45}$$

Before comparing the results of the numerical-integration-based solution technique with the results of the finite element method, the effect of the finite element mesh size on the natural frequency calculated by Nastran was investigated. Table 1 presents a sample convergence study that shows the nondimensional frequencies calculated by Eq. (45) for three different mesh sizes and the frequency calculated by the present method for the cylindrical-conical branched shell of revolution with a cone angle of 5°. In the convergence study, the circumferential wave number n was taken as 1. Table 1 shows that the frequencies calculated by Nastran did not change significantly with the mesh size used in the finite element model. For this particular case, the modal frequency was about 475 Hz, and the differences between the natural frequencies obtained by different mesh sizes are on the order of a few hertz.

In Fig. 4 good agreement is also observed between the present solution and the solution by Nastran for other cone angles. Both methods predicted similar variation of the fundamental natural frequency with the cone angle. It should be noted that in Fig. 4, the maximum difference between the Nastran results and the present solution is under 3%.

Sample Results on the Sphere–Cone Combination with Variable-Stiffness Coefficients

A sample analysis has been performed for the truncated sphere–cone combination shown in Fig. 5. The left part of the junction of the branched shell of revolution is a truncated sphere and the right part is a conical shell.

The particular sphere–cone combination is assumed to be manufactured by the filament-winding operation by starting the winding at the left end of the truncated sphere, and for the geodesic fiber path, the winding angle and the thickness along the shell axis are assumed to vary according to Eqs. (15) and (16), respectively. The particular sphere–cone combination is assumed to have the following geometric and material properties.

For the sphere, radius $R = 0.21$ m, $\phi_1 = 30°$, $\phi_2 = 70°$, and initial winding angle at the left end is 55°. For the cone, axial length $L = 0.315$ m, and cone angles are $\beta_c = 10$, 20, and 30°. The stacking sequence $[\theta/-\theta/\theta/-\theta/\theta/-\theta/\theta/-\theta/\theta/-\theta]_S$

Table 1 Variation of the nondimensional frequency W by the mesh size ($n = 1$ and $\beta_c = 5°$)

Number of nodes	Number of elements	Nastran solution	Present solution
3,616	1,184	0.5870	0.5987
14,112	4,662	0.5885	0.5987
20,444	6,764	0.5888	0.5987

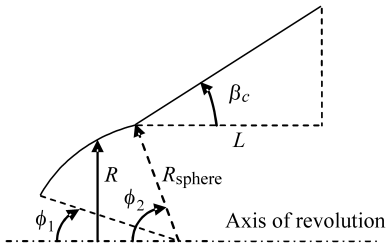

Fig. 5 Generator of the reference surface of the sphere–cone combination.

is symmetric with 24 layers, ply thickness is 0.24 mm at the starting edge of the initial winding, and ply materials are the same as in the cylinder–cone example.

For this particular example, continuity of the winding angle and the thickness is assumed at the junction. Figure 6 shows the variation of the winding angle and the normalized total shell thickness along the axis of the sphere–cone combination for three different cone angles β_c. In Fig. 6, the coordinate along the meridian of the shell is normalized separately with respect to the length of the meridian of the spherical and conical parts, and thicknesses are normalized with respect to the thickness at the left end of the spherical part, where the filament-winding operation is assumed to start.

It is seen from Fig. 6 that when the winding starts from the small radius edge of the spherical part, the winding angle and the thickness decreases along the meridian of the branched shell of revolution in accordance with Eqs. (15) and (16). For higher cone angles, the decrease in the winding angle and the thickness is higher in the conical part.

To demonstrate the effect of the variation of the winding angle and the thickness on the stiffness coefficients, variation of some of the stiffness coefficients along the meridian of the branched shell of revolution is shown in Fig. 7. Figure 7 gives the variation of the normalized extensional stiffness coefficients A_{ij} and normalized bending stiffness coefficients D_{ij} with respect to the normalized meridian of the sphere–cone combination.

In Fig. 7 extensional stiffness coefficients are normalized with respect to the value of A_{11}, and bending stiffness coefficients are normalized with respect to the value of D_{11} at the small radius edge of the spherical shell. Stiffness coefficients in the circumferential direction are drawn on logarithmic scale because of the sharp decrease of the circumferential stiffness coefficients (A_{22}, D_{22}) along the meridian of the branched shell of revolution. For the initial winding angle of 55°, it is observed that except for the extensional stiffness coefficient in the meridional direction (A_{11}), the stiffness coefficients decrease along the whole meridian of the branched shell of revolution. It should be noted that for a fixed shell-wall thickness at the starting edge of the filament-winding operation, the variation of the stiffness coefficients is strongly related to the initial winding angle and the starting edge of the winding. It is also noted from Fig. 7 that when the cone angle is increased, in accordance with the variation of the winding angle and the thickness, the decrease in the stiffness coefficients along the meridian of the conical shell is higher.

By incorporating the variation of the stiffness coefficients and thickness in the coefficient matrices of Eqs. (20) and (21), free-vibration analysis of the sphere–cone combination has been performed. The branched shell of revolution is assumed to be clamped at the small radius edge of the spherical part and free at the large-radius end of the conical part. Figure 8 shows the variation of the scaled nondimensional fundamental natural frequency [Eq. (45)] of the sphere–cone combination with respect to circumferential wave number for three different cone angles β_c.

The results in Fig. 8 are presented for the nonaxisymmetric vibration modes, and it is observed that at high circumferential wave numbers, the natural frequency of the branched shell of revolution with a lower cone angle is also higher. This behavior is attributed to the dominance of the bending strain-energy contribution to the total strain energy at high circumferential wave numbers [26]. At high circumferential wave numbers, circumferential slices of the shell

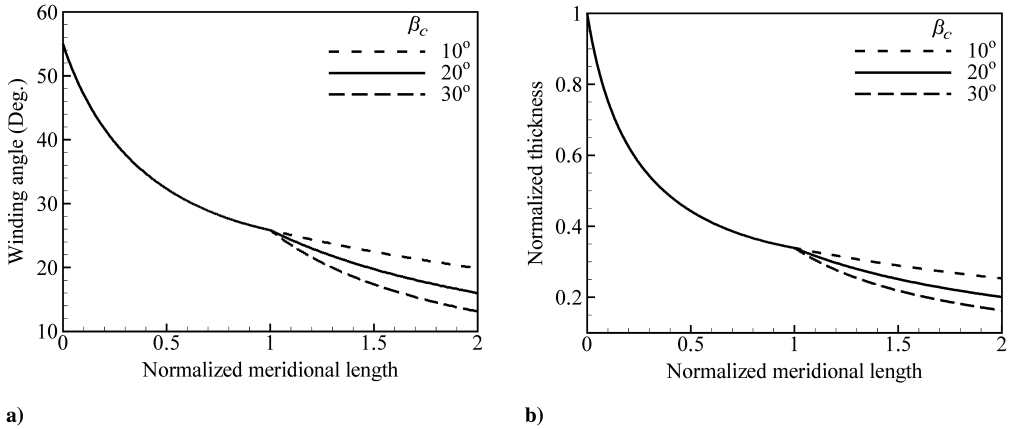

Fig. 6 Variation of winding angle and thickness along the axis of sphere–cone combination.

essentially behave like a beam under circumferential bending, and the bending stiffness coefficient in the circumferential direction (D_{22}) predominantly governs the magnitude of the natural frequency. It is deemed that higher circumferential bending stiffness and the shorter distance between the nodal meridians in the conical part of the branched shell of revolution with a lower cone angle account for the increase of the natural frequency at high circumferential wave numbers. It can also be deduced from Fig. 8 that at high circumferential wave numbers, the effect of the stiffness becomes more dominant on the natural frequencies, compared with the effect of the inertia. Although the conical part of the branched shell of revolution with a lower cone angle has higher thickness, and this implies higher inertia, the natural frequencies of the low-cone-angle branched shell are still higher at high circumferential wave numbers. At low circumferential wave numbers, extensional strain energy is more dominant in its contribution to the total strain energy [26], and it should be expected that the extensional stiffness coefficients become more dominant on the natural frequencies. For the beam vibration mode ($n = 1$) of the branched shell of revolution, natural frequency of the lower-cone-angle shell (which has higher extensional stiffness coefficients in the conical part) is higher. This conclusion supports the dominance of the extensional strain energy at low circumferential vibration modes. However, because the geometries of the branched shells of revolution are different due to the different cone angles of the conical part, a general statement cannot be made with regard to the effect of the extensional stiffness coefficients on the natural frequencies at low circumferential wave numbers.

For the sphere–cone combination, the normalized fundamental lateral-displacement mode shape (w^0), which is obtained through the recursive relation equations (38–44), is plotted in Fig. 9 for two different cone angles and for a circumferential wave number of 4. Figure 9 shows the cosine and sine parts of the Fourier transform of

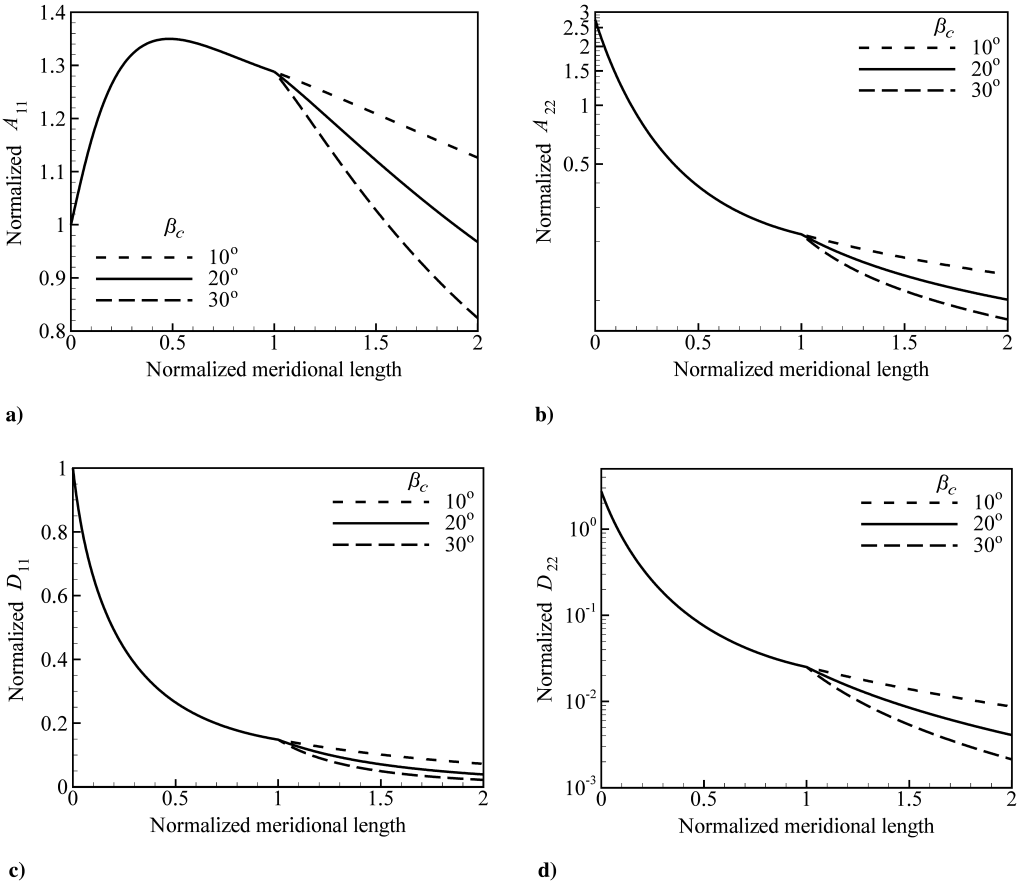

Fig. 7 Variation of stiffness coefficients of the sphere–cone combination for different cone angles.

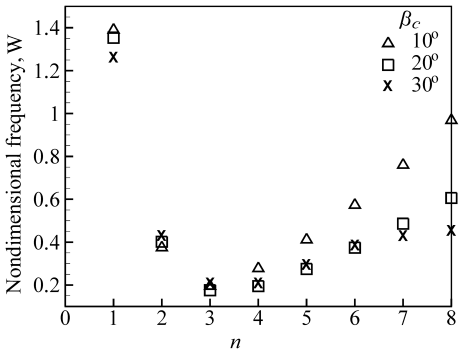

Fig. 8 Natural frequency versus circumferential wave number for different cone angles (β_c).

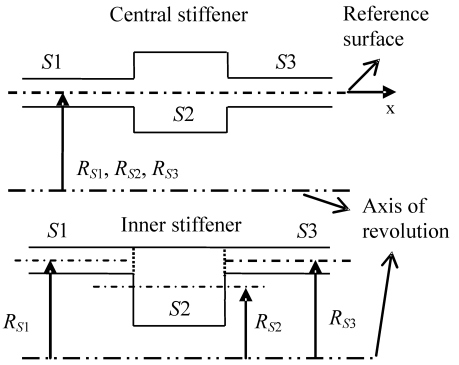

Fig. 10 Stiffener configurations.

the lateral displacement, and the effect of the branching is clearly seen at the junction of the spherical and conical part.

Because of the anisotropic nature of the shell-wall layup, the sine and cosine components of the Fourier transform of the lateral displacement are both nonzero. However, the sine component of the lateral displacement is very small compared with the cosine part, especially for the cone angle of 20°. It should be noted that at the junction, all the fundamental variables are calculated twice from Eq. (27). For the cone angle of 20°, the reference surfaces of the spherical and conical parts of the branched shell of revolution are tangent to each other at the junction ϕ_j. Therefore, there is no kink in the lateral displacement. For the cone angle of 30°, since the reference surfaces of the spherical and conical parts of the branched shell of revolution do not have a common tangent at the junction, there is a little jump in the lateral displacement at the junction due to the definition of the fundamental variables with respect to two different reference surfaces. Once the cosine and sine parts of the Fourier transform of the fundamental lateral displacement are determined, the actual lateral-displacement mode shape can be constructed using the complex Fourier series representation of the lateral displacement given by Eq. (11) in conjunction with Eq. (8) for the particular circumferential wave number.

Extension of the Numerical Integration Technique to Ring-Stiffened Shells of Revolution

In this section, application of the numerical integration technique is demonstrated for free-vibration analysis of filament-wound shells of revolution with ring stiffeners. To aid the understanding of the nomenclature used in the ring-stiffened shells of revolution, Fig. 10 shows central-stiffener and inner-stiffener configurations for the cylindrical shell geometry. Outer-stiffener configuration is similar to the inner-stiffener configuration, with the stiffener placed on the outer surface of the shell rather than on the inner surface.

In Fig. 10, $S1$ and $S3$ denote the shell regions without any stiffener, and $S2$ denotes the shell region with an integral stiffener that is assumed to be perfectly bonded to the shell wall. In the current study, ring stiffeners are modeled as shell segments. For the central stiffener configuration, the effect of the ring stiffener is integrated into the analysis by expressing the fundamental system of equations, given by Eq. (12), separately for the distinct shell regions with and without the stiffener. Fundamental shell variables are defined with respect to the common reference surface of the shell and the ring stiffener. For the stiffened part, the coefficient matrix K of Eq. (12) is modified by updating the laminate stiffness coefficients and thickness pertaining to the ring stiffener. The solution for the natural frequencies and the mode shapes then follows the same procedure as in branched shells of revolution. However, due to the use of the common reference surface for the shell and the ring stiffener, there is no need for transforming the fundamental shell variables at the shell-stiffener junction unless the stiffener corresponds to a branch point.

It is expected that for thicker ring stiffeners, the effect of different stiffener configurations on the natural frequencies of ring-stiffened shells of revolution would be higher. Therefore, a methodology is needed to incorporate different-configuration ring stiffeners into the free-vibration analysis. In this study, two methods are proposed for the inclusion of outer- and inner-stiffener configurations into the numerical-integration-based free-vibration analysis. These methods are called the fundamental variable-transformation method and common reference surface method.

Fundamental Variable-Transformation Method

In this approach, the fundamental shell variables are defined with respect to the reference surfaces of distinct shell regions with and without the ring stiffeners. Figure 11 shows the fundamental variables that are defined with respect to the midsurface of the shell regions with and without stiffener. It should be noted that the choice of the midsurface as the reference surface is quiet arbitrary and, in theory, any surface can be selected as the reference surface. However, the choice of midsurface is convenient to demonstrate the application of the fundamental variable-transformation method. In Fig. 11 positive directions of the fundamental shell variables are shown, and

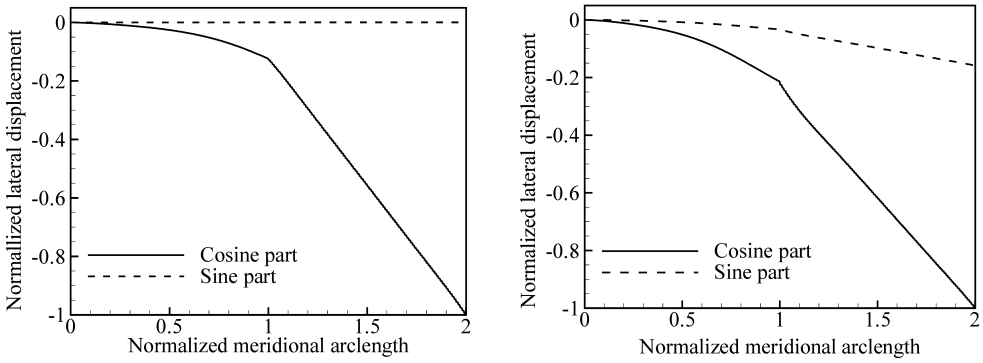

a) $\beta_c = 20°$ **b) $\beta_c = 30°$**

Fig. 9 Fundamental lateral-displacement mode shape for the sphere–cone combination ($n = 4$).

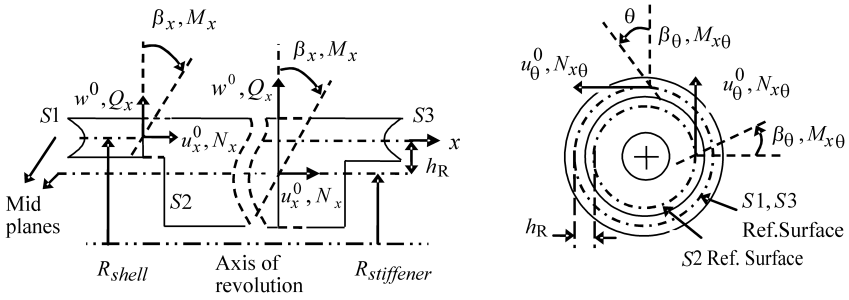

Fig. 11 Fundamental variables of shell regions with and without stiffener.

h_R denotes the offset between the reference surfaces of the shell walls with and without stiffener. For the stiffened region, it is assumed that stiffener thickness plus the shell-wall thickness is the total shell thickness at that region. It should be noted that for the inner-stiffener configuration, the radius of the midplane of the stiffener is given by $R_{\text{stiffener}} = R_{\text{shell}} - h_R$, and for the outer-stiffener configuration, the radius of the midplane of the stiffener is given by $R_{\text{stiffener}} = R_{\text{shell}} + h_R$.

In this method, at the shell-stiffener junctions, the fundamental variables are transformed by using the following relations. Fundamental variables that are preserved at the shell-stiffener junctions are w^0, β_x, β_θ, Q_x, N_x, and $N_{x\theta}$.

Inner-stiffener case, $S1$–$S2$ junction:

$$(u_x^0)_{S2} = (u_x^0)_{S1} - h_R(\beta_x)_{S1} \qquad (u_\theta^0)_{S2} = (u_\theta^0)_{S1} - h_R(\beta_\theta)_{S1}$$
$$(M_x)_{S2} = (M_x)_{S1} + h_R(N_x)_{S1} \qquad (M_{x\theta})_{S2} = (M_{x\theta})_{S1} + h_R(N_{x\theta})_{S1} \tag{46}$$

Inner-stiffener case, $S2$–$S3$ junction:

$$(u_x^0)_{S3} = (u_x^0)_{S2} + h_R(\beta_x)_{S2} \qquad (u_\theta^0)_{S3} = (u_\theta^0)_{S2} + h_R(\beta_\theta)_{S2}$$
$$(M_x)_{S3} = (M_x)_{S2} - h_R(N_x)_{S2} \qquad (M_{x\theta})_{S3} = (M_{x\theta})_{S2} - h_R(N_{x\theta})_{S2} \tag{47}$$

Outer-stiffener case, $S1$–$S2$ junction:

$$(u_x^0)_{S2} = (u_x^0)_{S1} + h_R(\beta_x)_{S1} \qquad (u_\theta^0)_{S2} = (u_\theta^0)_{S1} + h_R(\beta_\theta)_{S1}$$
$$(M_x)_{S2} = (M_x)_{S1} - h_R(N_x)_{S1} \qquad (M_{x\theta})_{S2} = (M_{x\theta})_{S1} - h_R(N_{x\theta})_{S1} \tag{48}$$

Outer-stiffener case, $S2$–$S3$ junction:

$$(u_x^0)_{S3} = (u_x^0)_{S2} - h_R(\beta_x)_{S2} \qquad (u_\theta^0)_{S3} = (u_\theta^0)_{S2} - h_R(\beta_\theta)_{S2}$$
$$(M_x)_{S3} = (M_x)_{S2} + h_R(N_x)_{S2} \qquad (M_{x\theta})_{S3} = (M_{x\theta})_{S2} + h_R(N_{x\theta})_{S2} \tag{49}$$

Depending on whether the ring stiffener is an inner or outer stiffener, and depending on the location of the shell-stiffener junction (shell-stiffener:$S1$–$S2$, stiffener shell:$S2$–$S3$), transformation matrices can be defined at each junction by using the relations given by Eqs. (46–49). Thus, the transformation relations in partitioned form can be written at the shell-stiffener or stiffener-shell junctions in the same manner as in Eq. (22) or Eq. (24). It should be noted that the transformation matrices defined at the shell-stiffener and stiffener-shell junctions are different for the displacements and stress/moment resultants, and this is clearly seen from Eqs. (46–49). Therefore, it would be appropriate to modify Eq. (22) as shown in Eq. (50):

$$\{\psi^{(1)}(\phi_j)\}_{S2} = [\text{TR}]^1_{10\times10}\{\psi^{(1)}(\phi_j)\}_{S1}$$
$$\{\psi^{(2)}(\phi_j)\}_{S2} = [\text{TR}]^2_{10\times10}\{\psi^{(2)}(\phi_j)\}_{S1} \tag{50}$$

where $[\text{TR}]^1$ is the transformation matrix that relates the displacements and rotations at the shell-stiffener or stiffener-shell junctions, and $[\text{TR}]^2$ is the transformation matrix that relates the stress and moment resultants at the shell-stiffener or stiffener-shell junctions. Following the definition of new transformation matrices, Eqs. (23–44) would have to be modified appropriately by distinguishing the new matrices $[\text{TR}]^1$ and $[\text{TR}]^2$. As long as the transition matrices E_Z and C_Z in Eq. (27) are defined appropriately at each junction, the remaining solution procedure is exactly same as the solution for a branched shell of revolution.

Common Reference Surface Method

In the common reference surface method, the midsurface of the shell wall (which is denoted by R_{shell} in Fig. 11) is also used as the reference surface for the ring stiffener. All the fundamental variables are defined with respect to this common reference surface. Since all the fundamental variables of the shell regions with and without the ring stiffeners are defined with respect to the common reference surface, as long as the stiffener edges do not coincide with a junction where the shell branches to a different type, no transformation of the fundamental variables is necessary at the shell-stiffener junctions. Therefore, for the inner- and outer-stiffener configurations to reflect the changes in the stiffness coefficients and the thickness of the shell regions with and without the ring stiffener, the only action that needs to be taken is the modification of the coefficient matrix K in Eq. (18) by defining appropriate stiffness coefficients and thickness for the shell wall and the stiffeners. It should be noted that in this method, while calculating the stiffness coefficients for the inner- and outer-stiffener configurations, definitions of the layer positions should be made accordingly by taking the midplane of the main shell wall as the reference surface. The positive direction of the lateral displacement is outward and therefore any layer position measured toward the axis of the shell of revolution from the midplane of the shell wall is taken as negative, whereas layer position measured outward from the midplane of the shell wall is taken as positive. Thus, in this method, the offset distance h_R is implicitly taken care of while calculating the stiffness coefficients.

Comparison of the Methods

To demonstrate the applicability of both methods in the free-vibration analysis of macroscopically anisotropic ring-stiffened shells of revolution, a sample study has been performed for a cylindrical shell with the following geometric and material properties and stiffener configurations.

Geometric properties are cylinder length L of 1.2 m, radius of the reference surface of the shell with no stiffener(R_{S1}, R_{S3}) of 0.21 m, shell-wall thickness without stiffener of 1.92 mm, shell-wall thickness with stiffener of 5.76 mm, and stiffener width of 60 mm. Ply material properties are high-modulus graphite epoxy; $E_1 =$ 207.348 GPa, $E_2 = 5.183$ GPa, $G_{12} = G_{23} = G_{13} = 3.11$ GPa, $\nu_{12} = 0.25$, and $\rho = 1524.474\ \text{kg m}^{-3}$; thickness is 0.24 mm; shell wall without stiffener consists of eight plies with 50° fiber orientation; and shell wall with stiffener consists of 24 plies with 50° fiber orientation. The inner- and outer-stiffener configurations have a single stiffener placed at the midspan. For the boundary condition, the shell is clamped at the left end ($x = 0$) and simply supported at the right end ($x = L$).

Comparison of the natural frequencies [Eq. (45)] determined by the fundamental variable-transformation method and common reference surface method is made in Table 2. For the inner- and outer-

Table 2 Comparison of the scaled nondimensional frequencies *W*

	Inner stiffener		Outer stiffener	
n	Ref. surface	Variable trans.	Ref. surface	Variable trans.
0	0.4746	0.4744	0.4757	0.4753
1	0.3583	0.3581	0.3587	0.3585
2	0.1626	0.1628	0.1575	0.1576
3	0.1687	0.1697	0.1541	0.1543
4	0.2406	0.2413	0.2252	0.2254
5	0.3297	0.3303	0.3163	0.3166
6	0.4310	0.4317	0.4209	0.4214
7	0.5394	0.5399	0.5331	0.5336

Table 3 Modal frequencies (rad/s) of inner-stiffener configuration

Stiffener thickness	Present study	[15]
1 cm	720.6	723.4
2 cm	717.9	721.0

stiffener configurations, Table 2 lists the scaled fundamental nondimensional natural frequencies corresponding to different circumferential wave numbers. As expected, the results of both approaches are very close to each other for both inner- and outer-stiffener configurations. It should be noted that in the common reference surface method, for a symmetric stacking sequence with respect to the midsurface of the ring stiffener, bending-stretching coupling coefficients will be nonzero in the stiffener region because of the offset of the reference surface from the midsurface of the ring stiffener. On the other hand, in the fundamental variable-transformation method, for symmetric stacking sequence with respect to the midsurface of the shell wall with and without the ring stiffener, the bending-stretching coupling coefficients vanish. It is deemed that both methods can be used in the analysis of ring-stiffened anisotropic shells of revolution. However, fundamental variable-transformation method requires the definition of additional transformation matrices for the fundamental variables at each shell-stiffener or stiffener-shell junction.

Verification Study

To verify the applicability of the fundamental transformation and common reference surface methods described above, results of the present study have been compared with the results of Wang and Lin [15], who performed an analytic study to calculate the modal frequencies and mode shapes of a ring-stiffened symmetric cross-ply $[90^\circ/0^\circ/90^\circ]_s$ cylindrical shell with the following properties.

Geometric properties are a cylinder length of 5 m, radius of the shell of 0.3 m, and shell-wall thickness of 3 cm. Ply material is graphite epoxy; $E_1 = 150$ GPa, $E_2 = 9$ GPa, $G_{12} = G_{13} = 7.1$ GPa, $G_{23} = 2.5$ GPa, $\nu_{12} = 0.3$, and $\rho = 1600$ kg/m^3. Inner-stiffener configuration has a single stiffener placed at the midspan. Ring stiffeners are made of aluminum 6061-T6 with $E_1 = 70$ GPa and $G = 26$ GPa. The boundary condition is a shell clamped at both ends.

For comparison, modal frequencies for the inner-stiffener configuration are calculated for two different stiffener thicknesses (1 and 2 cm) and for a stiffener width of 3 cm. Table 3 compares the fundamental modal frequencies for the beam mode of vibration $n = 1$. Frequency results used in the comparison are taken from Table 3 of [15] for the inner ring configuration. It should be noted that for the particular ring-stiffened shell configuration studied by Wang and Lin [15], modal frequencies of the inner and outer ring-stiffener configurations were almost equal to each other.

Table 3 shows that the frequencies calculated by both studies are very close to each other and the frequency trends, with respect to change in the stiffener thickness, are also similar. In the present study, fundamental variable transformation and common reference surface methods both gave almost the same results for the stiffened shell configuration studied.

Analysis of Ring-Stiffened Shells of Revolution with Variable Winding Angle and Thickness

Common reference surface method is used to demonstrate the application of the numerical-integration-based free-vibration analysis for ring-stiffened filament-wound conical shells of revolution considering the variation of the winding angle and the thickness along the meridian of the shell. Figure 12 shows the shell wall of the variable-thickness conical shell that is assumed to be manufactured by the filament-winding operation, such that the winding angle and the thickness vary according to Eqs. (15) and (16), respectively. The ring stiffener is assumed to be secondarily bonded to the filament-wound conical shell, and in the present study, a constant-thickness ring stiffener is considered. It is also assumed that the stiffener is composed of several composite layers with constant fiber orientation. However, in the numerical-integration-based analysis, inclusion of variable-thickness and variable-stiffness ring stiffeners into the problem brings about no difficulty, since the ring stiffeners are modeled as shell segments. Figure 12 shows that the midsurface of the shell wall is taken as the common reference surface with respect to which all the fundamental variables of the conical shell and the ring-stiffener region are defined.

In the present study, a computer code is prepared such that any number of ring stiffeners with specified widths at any axial location can be included in the governing equations automatically. A sample study has been performed for a conical shell with the following geometric, material properties, and stiffener configurations.

Geometric properties are the slant length SL of the cone of 0.7 m; cone angle β_c of 20°; radius of the reference surface of the conical shell at the narrow end, where the winding is assumed to start, of 0.2 m; initial shell-wall thickness at the narrow end of 1.92 mm; constant wall thickness of the ring stiffener (excludes the shell-wall thickness) of 5.76 mm; and stiffener width of 50 mm.

For ply material properties, the same material are used as for the shell wall and the ring stiffeners; Young's modulus in the fiber direction is $E_1 = 213.74$ GPa; Young's modulus transverse to fiber is $E_2 = 18.62$ GPa, shear moduli are $G_{12} = G_{13} = 5.171$ GPa and $G_{23} = 4.137$ GPa; Poisson's ratio is $\nu_{12} = 0.28$; and mass density is $\rho = 2051.88$ kg/m^3.

Shell-wall ply properties are a ply thickness of the conical shell wall of 0.24 mm at the narrow end, where the winding operation is assumed to start, and a shell wall without the ring stiffener consists of eight plies with 35° fiber orientation at the starting edge of the winding.

Ring-stiffener ply properties are a fiber orientation angle of each layer of 20°, and a stacking sequence of the ring stiffener of $[\theta/-\theta/\theta/-\theta/\theta/-\theta/\theta/-\theta/\theta/-\theta]_S$ symmetric with 24 layers with a ply thickness of 0.24 mm. The inner-stiffener configuration with one, two, and three stiffeners is placed at axial locations such that the total shell length is divided into equal length segments in each case. The boundary conditions are that the shell is clamped at the narrow end and clamped and free at the wide end.

Figures 13 and 14 give the variation of the scaled nondimensional fundamental natural frequency with respect to the circumferential wave number for different numbers of stiffeners and for the

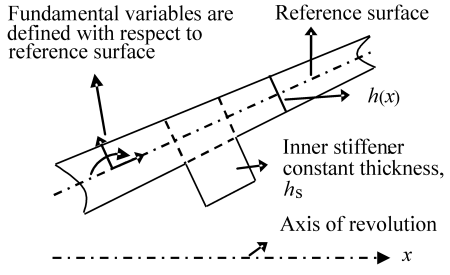

Fig. 12 Variable-thickness filament-wound conical shell with ring stiffener.

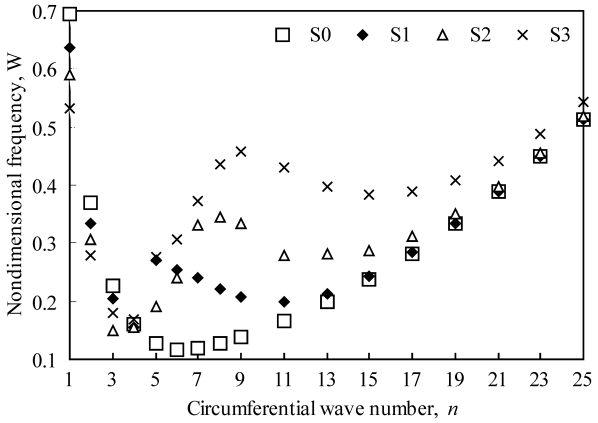

Fig. 13 Fundamental frequency versus circumferential wave number: clamped–free.

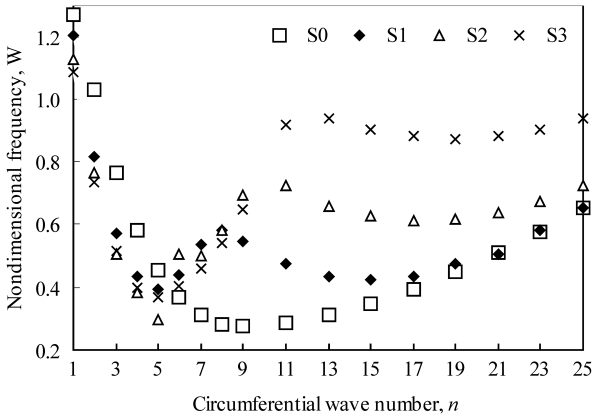

Fig. 14 Fundamental frequency versus circumferential wave number: clamped–clamped.

no-stiffener case. In Figs. 13 and 14, S0 denotes the shell without any stiffener and, similarly, S1, S2 and S3 denote shells with one, two, and three ring stiffeners, respectively. The natural frequencies plotted in Figs. 13 and 14 correspond to the nonaxisymmetric lateral-displacement modes of the truncated conical shell.

The common behavior that is observed for both edge conditions is that the effect of increasing the number of ring stiffeners along the shell axis is felt more at higher circumferential vibration modes. This behavior is again attributed to the dominance of bending strain energy at high circumferential wave numbers. At high circumferential vibration modes, circumferential slices of the shell of revolution behave as beams under circumferential bending and the natural frequencies increase when the number of ring stiffeners is increased. However, at low circumferential wave numbers, extensional strain energy is more dominant in its contribution to the total strain energy, and it is deemed that due to the additional mass effect of the stiffeners, natural frequency decreases when the number of ring stiffeners is increased. It is also noted that when the circumferential wave number is increased further, the natural frequencies of shells with different numbers of stiffeners and with no stiffener gradually merge together. This behavior is more clearly seen for the clamped–free edge condition in the circumferential wave number range analyzed. Physically, a high circumferential wave number means many nodal points around the circumference. Therefore, beyond a certain number of nodal points around the circumference, the effect of the number of stiffeners on the frequencies is felt less and frequencies start to merge together. Another observation from Figs. 13 and 14 is that for conical shells with ring stiffeners, there is a local peak in the natural frequencies at an intermediate circumferential wave number, and such a local peak does not exist for the shell with no ring stiffener. It is observed that the local peak shifts toward higher circumferential wave numbers as the number of ring stiffeners is increased for both edge conditions.

For both edge conditions, Figs. 15 and 16 show the cosine part of the Fourier transform of the fundamental mode shape of the conical shell corresponding to the lateral displacement w^0 for $n = 3$. Since the sine part of the lateral displacement turned out to be very small compared with the cosine part, the sine part is not shown; therefore, the cosine part depicts almost the actual variation of the lateral displacement. Figures 15 and 16 show the mode shapes for the no-stiffener and the single inner-stiffener configuration at the midspan of the conical shell.The mode shapes shown in Figs. 15 and 16 are obtained such that the variation of the winding angle and the thickness of the main shell wall according to Eqs. (15) and (16) are included in the analysis. For this particular stiffener configuration, it is observed that the ring stiffener primarily affects the mode shape around the region where it is attached. It is also observed from Fig. 16 that for the conical shell that is clamped at both edges, the peak displacement point shifts toward the large-radius end for the no-stiffener case. This shift can be attributed to the cone geometry and also to the decrease of the stiffness coefficients and thickness along the axis of the filament-wound conical shell when the winding starts from the small radius end. It should be expected that at higher circumferential vibration modes, the peak displacement point would move toward the large-radius edge even more. This is because at high circumferential wave numbers, circumferential slices of the shell essentially behave like a beam under circumferential bending, and a slice taken from a section close to the larger end of the cone resembles a longer span beam compared with a slice taken from a section close to the smaller end. The attachment of a ring stiffener at the midspan of the conical shell is seen to slightly shift the peak displacement point toward the midspan.

Figure 17 shows the effect of the variation of winding angle and the thickness on the natural frequencies of the conical shell. In Fig. 17 VS

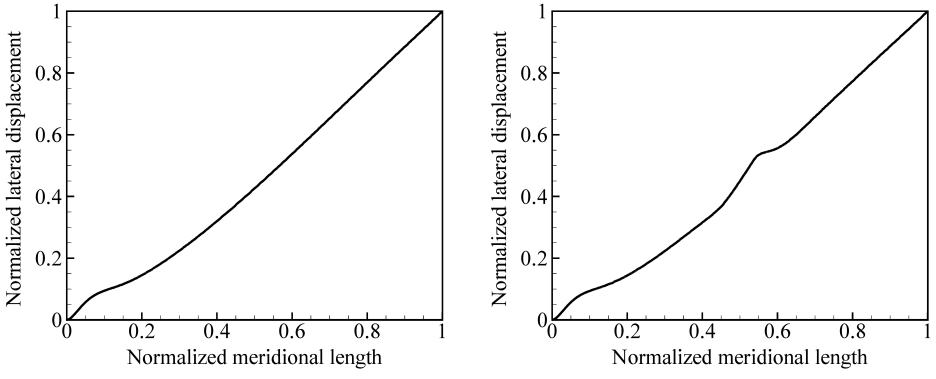

a) **b)**

Fig. 15 Fundamental lateral-displacement mode shape ($n = 3$), clamped–free: a) no stiffener and b) single stiffener at midspan.

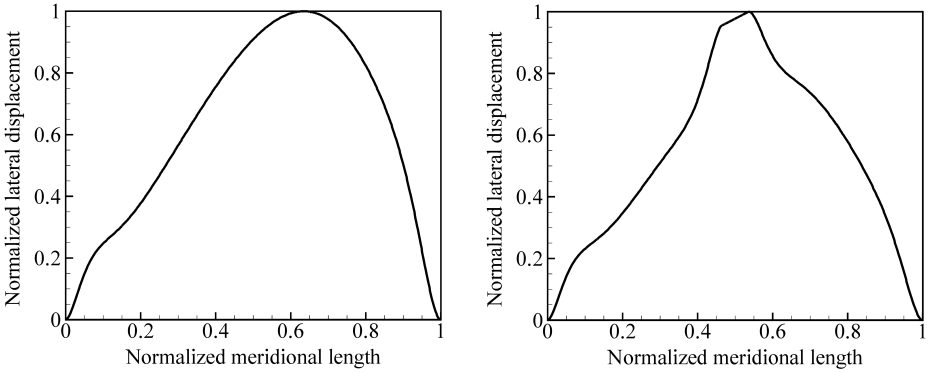

a) b)

Fig. 16 Fundamental lateral-displacement mode shape ($n = 3$), clamped–clamped: a) no stiffener and b) single stiffener at midspan.

stands for the variable-stiffness case, in which the winding angle and the thickness continuously vary along the meridian of the shell, and CS stands for the constant-stiffness case, in which the initial winding angle and thickness at the starting edge of the winding operation are assumed to be constant throughout the shell. The results are obtained for a single-stiffener case at the midspan.

At lower circumferential wave numbers, natural frequencies of the variable-stiffness case are higher compared with the frequencies of the constant-stiffness case. This behavior is attributed to the combined effect of the variable-stiffness and variable inertia of the conical shell with varying winding angle and thickness. The stiffness coefficients and the thickness of the variable-stiffness case decrease along the meridian of the conical shell, and for this particular symmetric shell-wall layup, the bending-stretching coupling coefficients vanish for both cases. However, some of the other coupling stiffness coefficients with subscripts 16 and 26 in Eq. (3) and subscript 45 in Eq. (4) do not vanish for the particular shell-wall layup, and for the constant-stiffness case, the nonzero coupling stiffness coefficients are higher over the span of the shell compared with the coupling stiffness coefficients of the variable-stiffness case. The lower natural frequency of the constant-stiffness case can be attributed to the higher inertia due to the assumption of constant thickness and also to the flexibility of the shell due to the existence of higher coupling stiffness coefficients compared with the variable-stiffness case. It should be noted that at low circumferential wave numbers, the bending strain-energy contribution to the total strain energy is lower [26] and therefore the effect of bending stiffness coefficients on the natural frequencies is less. However, at high circumferential wave numbers, it is observed that the natural frequencies of the constant-stiffness case are considerably higher than the frequencies of the variable-stiffness case. The differences in the frequencies increase at higher circumferential vibration modes. This behavior is attributed to the dominance of the bending strain-energy contribution to the total strain energy at high circumferential wave numbers [26]. At high circumferential wave numbers, circumferential slices of the shell essentially behave like a beam under circumferential bending. Therefore, the bending stiffness coefficient in the circumferential direction (D_{22}) predominantly governs the magnitude of the natural frequency, and the constant-stiffness case has a higher bending stiffness coefficient in the circumferential direction compared with the variable-stiffness case. For the constant winding angle and thickness assumption, circumferential bending stiffness at the starting edge of the winding at the smaller end of the cone is taken as constant along the axis of the shell. However, Fig. 7 shows that for the variable-stiffness case, the circumferential bending stiffness coefficient drops toward the larger end of the cone.

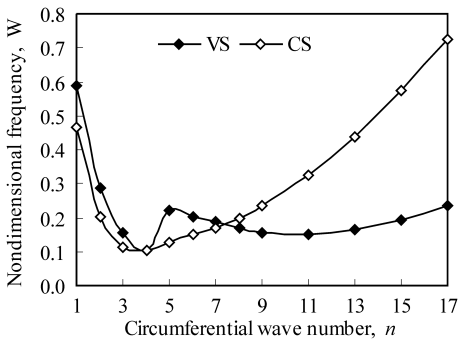

Fig. 17 Natural frequency versus circumferential wave number: single stiffener at midspan.

Conclusions

A methodology based on the numerical integration technique is presented for the free-vibration analysis of shear deformable filament-wound branched shells of revolution with ring stiffeners considering the variation of the winding angle and thickness along the meridian of the branched shell of revolution. For the filament-wound shells of revolution, filaments are assumed to be placed along the geodesic fiber path on the shell of revolution, resulting in the variation of the stiffness coefficients only along the meridian of the shell of revolution with general meridional curvature. Extension of the multisegment numerical integration technique to the free-vibration analysis of branched anisotropic shells of revolution is demonstrated. The applicability of the method of solution is further extended to the ring-stiffened filament-wound shells of revolution and two alternative methods of analysis are presented.

It has been shown that either by the fundamental variable-transformation method or by the common reference surface method, free-vibration analysis of shells of revolution with ring stiffeners, which are placed asymmetrically with respect to the middle surface of the shell, can be performed by the numerical-integration-based solution method. For the ring-stiffened shells of revolution, the use of a common reference surface for the main shell wall and the stiffener region is advantageous, because the transformation of the fundamental shell variables at the shell-stiffener junction can be eliminated. However, for shells of revolution with branches, the transformation of the fundamental variables has to be carried out at the junctions because of the change of the reference surface at the junctions.

It has also been shown that the effect of number of ring stiffeners on the fundamental natural frequencies is closely linked to the particular circumferential vibration mode. At low circumferential vibration modes, the natural frequencies of shells of revolution, reinforced by the ring stiffeners, are actually lower than the natural frequencies of shell of revolution that are not ring-stiffened.

The significant effect of the variation of the winding angle and the thickness of filament-wound ring-stiffened shells of revolution on the fundamental natural frequencies corresponding to different circumferential vibration modes has also been demonstrated for a truncated conical shell of revolution.

It is deemed that the numerical-integration-based methodology provides an alternative and powerful solution technique to analyze anisotropic shells of revolution with meridionally varying geometric

and material properties. The inclusion of discretely or continuously varying geometric and material properties along the meridian of the shell of revolution brings about no extra difficulty in the solution process.

Appendix: Transformation Matrix TR

The nonzero components of the transformation matrix TR are

$$\mathrm{TR}(1,1) = \mathrm{TR}(2,2) = \mathrm{TR}(3,3) = \mathrm{TR}(4,4)$$
$$= \mathrm{TR}(9,9) = \mathrm{TR}(10,10) = \cos\beta$$
$$\mathrm{TR}(5,5) = \mathrm{TR}(6,6) = \mathrm{TR}(7,7) = \mathrm{TR}(8,8) = 1;$$
$$\mathrm{TR}(1,3) = \mathrm{TR}(2,4) = -\sin\beta;$$
$$\mathrm{TR}(3,1) = \mathrm{TR}(4,2) = \sin\beta$$

References

[1] Springer, G. S., "Filament-Winding Process Model for Thermosetting Matrix Composites," *Advanced Composites Manufacturing*, edited by Timothy. G. Gutowski, Wiley, New York, 1997, pp. 373–393.

[2] Baruch, M., Arbocz, J., and Zhang, G. Q., "Laminated Conical Shells-Considerations for the Variations of the Stiffness Coefficients," *Proceedings of the 36th AIAA/ASME/ASCE/AHS/ASC Structures, Structural Dynamics, and Materials Conference*, AIAA, Reston, VA, 1994, pp. 2505–2516.

[3] Korjakin, A., Rikards, R., Chate, A., and Altenbach, H., "Analysis of Free Damped Vibrations of Laminated Composite Conical Shells," *Composite Structures*, Vol. 41, No. 1, 1998, pp. 39–47. doi:10.1016/S0263-8223(98)00024-5

[4] Goldfeld, Y., and Arbocz, J., "Buckling of Laminated Conical Shells Given the Variations of the Stiffness Coefficients," *AIAA Journal*, Vol. 42, No. 3, 2004, pp. 642–649. doi:10.2514/1.2765

[5] Park, J. S., Hong, C. S., Kim, C. G., and Kim, C. U., "Analysis of Filament Wound Composite Structures Considering the Change of Winding Angles Through the Thickness Direction," *Composite Structures*, Vol. 55, No. 1, 2002, pp. 63–71. doi:10.1016/S0263-8223(01)00137-4

[6] Noor, A. K., and Peters, J. M., "Vibration Analysis of Laminated Anisotropic Shells of Revolutions," *Computer Methods in Applied Mechanics and Engineering*, Vol. 61, No. 3, 1987, pp. 277–301. doi:10.1016/0045-7825(87)90096-X

[7] Xi, Z. C., Yam, L. H., and Leung, T. P., "Semi-Analytical Study of Free-Vibration of Composite Shells of Revolution Based on the Reissner-Mindlin Assumption," *International Journal of Solids and Structures*, Vol. 33, No. 6, 1996, pp. 851–863. doi:10.1016/0020-7683(95)00063-G

[8] Tan, D. Y., "Free-Vibration Analysis of Shells of Revolution," *Journal of Sound and Vibration*, Vol. 213, No. 1, 1998, pp. 15–33. doi:10.1006/jsvi.1997.1406

[9] Timarci, K. P., and Soldatos, K. P., "Vibrations of Angle-Ply Laminated Circular Cylindrical Shells Subjected to Different Sets of Edge Boundary Conditions," *Journal of Engineering Mathematics*, Vol. 37, Nos. 1–3, 2000, pp. 211–230. doi:10.1023/A:1004794513444

[10] Santos, H., Soares, C. M. M., Soares, C. A. M., and Reddy, J. N., "A Semi-Analytical Finite Element Model for the Analysis of Laminated 3D Axisymmetric Shells: Bending, Free-Vibration and Buckling," *Composite Structures*, Vol. 71, Nos. 3–4, 2005, pp. 273–281. doi:10.1016/j.compstruct.2005.09.006

[11] Kayran, A., and Yavuzbalkan, E., "Semi-Analytical Study of Free-Vibration Characteristics of Shear deformable Filament Wound Anisotropic Shells of Revolution," *Journal of Sound and Vibration*, Vol. 319, Nos. 1–2, 2009, pp. 260–281. doi:10.1016/j.jsv.2008.05.024

[12] Sivadas, K. R., and Ganesan, N., "Free-Vibration Analysis of Combined and Stiffened Shells," *Computers and Structures*, Vol. 46, No. 3, 1993, pp. 537–546. doi:10.1016/0045-7949(93)90223-Z

[13] Ruotolo, R., "A Comparison of Some Thin Shell Theories Used for the Dynamic Analysis of Stiffened Cylinders," *Journal of Sound and Vibration*, Vol. 243, No. 5, 2001, pp. 847–860. doi:10.1006/jsvi.2000.3447

[14] Xiang, Y., Ma, Y. F., Kitipornchai, S., Lim, C. W., and Lau, C. W. H., "Exact Solutions for Vibration of Cylindrical Shells with Intermediate Ring Supports," *International Journal of Mechanical Sciences*, Vol. 44, No. 9, 2002, pp. 1907–1924. doi:10.1016/S0020-7403(02)00071-1

[15] Wang, R. T., and Lin, Z. X., "Vibration Analysis of Ring-Stiffened Cross-Ply Laminated Cylindrical Shells," *Journal of Sound and Vibration*, Vol. 295, Nos. 3–5, 2006, pp. 964–987. doi:10.1016/j.jsv.2006.01.061

[16] Pan, Z., Li, X., and Ma, J., "A Study on Free-Vibration of a Ring Stiffened Thin Circular Cylindrical Shell with Arbitrary Boundary Conditions," *Journal of Sound and Vibration*, Vol. 314, Nos. 1–2, 2008, pp. 330–342. doi:10.1016/j.jsv.2008.01.008

[17] Kalnins, A., "Free-Vibration of Rotationally Symmetric Shells," *Journal of the Acoustical Society of America*, Vol. 36, No. 7, 1964, pp. 1355–1365. doi:10.1121/1.1919208

[18] Reissner, E., "A New Derivation of the Equations for the Deformation of Elastic Shells," *American Journal of Mathematics*, Vol. 63, No. 1, 1941, pp. 177–184. doi:10.2307/2371288

[19] Yavuzbalkan, E., "Free-Vibration Analysis of Anisotropic Laminated Composite Shells of Revolution," M.Sc. Thesis, Dept. of Aerospace Engineering, Middle East Technical Univ., Ankara, Turkey, 2005.

[20] Soedel, W., *Vibration of Shells and Plates*, Marcel Dekker, New York, 1993, Chaps. 2,3,12,15.

[21] Toorani, M. H., and Lakis, A. A., "General Equations of Anisotropic Plates and Shells Including Transverse Shear Deformations, Rotatory Inertia and Initial Curvature Effects," *Journal of Sound and Vibration*, Vol. 237, No. 4, 2000, pp. 561–615. doi:10.1006/jsvi.2000.3073

[22] Vinson, J. R., and Sierakowski, R. L., *The behavior of Structures Composed of Composite Materials*, Kluwer Academic, Dordrecht, The Netherlands, 2002, Chap. 2.

[23] Whitney, J. M., "The Effect of Transverse Shear Deformation on the Bending of Laminated Plates," *Journal of Composite Materials*, Vol. 3, No. 3, 1969, pp. 534–547. doi:10.1177/002199836900300316

[24] Mindlin, R. D., "Influence of Rotatory Inertia and Shear on Flexural Motions of Isotropic, Elastic Plates," *Journal of Applied Mechanics*, Vol. 18, No. 1, 1951, pp. 31–38.

[25] Schaeffer, H. G., *MSC. Nastran Primer for Linear Static Analysis*, MSC Software Corp., Santa Ana, CA, 2001, pp. 200–201.

[26] Arnold, R. N., and Warburton, G. B., "Flexural Vibrations of the Walls of Thin Cylindrical Shells Having Freely Supported Ends," *Proceedings of the Royal Society of London, Series A: Mathematical and Physical Sciences*, Vol. 197, No. 1049, 1949, pp. 238–256. doi:10.1098/rspa.1949.0061

R. Kapania
Associate Editor